Comparison of Mutual Information–Based Warping Accuracy for Fusing Body CT and PET by 2 Methods: CT Mapped onto PET Emission Scan Versus CT Mapped onto PET Transmission Scan

Joseph Skalski[1]; Richard L. Wahl, MD[1]; and Charles R. Meyer, PhD[2]

[1]*Department of Nuclear Medicine and Radiology, Johns Hopkins University, Baltimore, Maryland;* *and* [2]*Department of Radiology, University of Michigan Medical Center, Ann Arbor, Michigan*

This article assesses the resulting accuracies of 2 registration methods using the same multimodal mutual information registration algorithm. In the indirect, fusion method, the CT dataset is warped onto the PET transmission scan, and then the patient's attenuation-corrected emission dataset is substituted for the transmission dataset. In the direct, fusion method, the CT is warped directly onto the attenuation-corrected emission dataset. **Methods:** CT and ^{18}F-FDG PET image datasets from 14 subjects with malignant lesions in the thorax were registered. In both CT and PET imaging acquisitions, the patient's arms were at the patient's side, resting on the scanning couch in a manner similar to that of routine PET acquisition procedures. The accuracy of the 2 warping registrations was assessed by measuring the distance between lesion centroids on CT and PET emission after fusion. **Results:** The indirect method has a statistically smaller mean error, 6.2 mm, than the direct method, 10.6 mm. **Conclusion:** The indirect method appears to be the more accurate/reliable choice for fusing body CT and FDG PET.

Key Words: registration; fusion; mutual information; CT; PET; emission; transmission; lesion centroids

J Nucl Med 2002; 43:1184–1187

Fusion of functional and anatomic imaging methods, such as PET and CT, is assuming growing importance in medical practice. Such fusion of anatometabolic images provides valuable information for patient management (*1*). Although there are several existing methods to perform multimodality warping to map one modality dataset into the geometry of another modality, there are few, if any, published direct validations of the various methods. Here "direct" is taken to mean a quantitative comparison between the results of the method with known truth. Most published validations are indirect, involving tests such as comparing the results across different methods where one of the methods may be an expert generating fiducials or segmentations (*2*,*3*). We present the results of a multimodality warping (i.e., warping the same patient's PET thoracic dataset onto their CT dataset), which is also an indirect validation in which the expert's role is limited to manual CT lesion segmentation. Lesion definition in PET emission datasets was computed automatically using a quantitative segmentation method based on intensities as described (*4*). The distance between the CT and PET lesion centroids was measured in the CT's geometry after the warping registration has been computed; centroids were computed using gray-scale weighting within the volume of interest (VOI). The gray-scale weighting can reduce potential bias resulting from the expert's selection of the CT VOI in that the position of the centroid depends not only on the VOI but also on the underlying Hounsfield values within the VOI. In all cases, the ideal distance between centroids after warping should be zero.

Received Nov. 9, 2001; revision accepted Apr. 26, 2002.

For correspondence or reprints contact: Charles R. Meyer, PhD, Department of Radiology, 3307 Kresge III Research Building, University of Michigan Medical Center, Ann Arbor, MI 48109-0553.

E-mail: cmeyer@umich.edu

MATERIALS AND METHODS

Subjects

Fourteen lung cancer subjects were studied with CT and ^{18}F-FDG PET as part of an Institutional Review Board–reviewed study evaluating the accuracy of PET for lung cancer staging. All but 2 of these subjects underwent PET and CT on the same day; the remaining 2 subjects had scans separated by 1 and 5 d. In this study, tumors of various sizes were examined, ranging from small focused lesions to large tumors with collapsed lungs.

PET imaging was preformed using a 921-EXACT PET camera (Siemens Medical Systems, Hoffman Estates, IL) with a 15-cm axial field of view. Two contiguous 10-min transmission acquisitions and attenuation-corrected emission acquisitions were reconstructed to a 128 × 128 × 47 matrix. The voxel size of the PET images was 4.21 × 4.21 × 3.38 mm. All of the PET scans were

TABLE 1
Results by Subject

Subject no.	Prior lung therapy	Time between PET and CT scans (d)	PET EM tumor volume (mm^3)	CT tumor volume (mm^3)	EM centroid loci by: Registration of TR scan*			EM centroid loci by: Direct registration of EM scan†			CT centroid (reference)			Centroid error regarding CT (mm)		Distance between methods A and B (mm)
					z (mm)	*y* (mm)	*x* (mm)	*z* (mm)	*y* (mm)	*x* (mm)	*z* (mm)	*y* (mm)	*x* (mm)	Method A	Method B	
1	None	0	225	626	−86.1	247.2	172.5	−92.4	246.7	172.2	−89.8	251.2	169.7	6.2	5.7	6.3
2	None	0	579	675	−75.0	25.1	−27.2	−75.0	21.7	−26.0	−80.2	24.5	−27.2	5.3	6.1	3.6
3	None	0	2,789	5,758	−117.8	246.9	163.8	−117.2	251.0	160.1	−115.6	230.9	167.9	16.7	21.6	5.5
4	None	0	5,708	5,951	−128.4	−40.4	74.7	−131.1	−39.3	72.8	−129.7	−39.8	77.0	2.6	4.4	3.5
5	None known	0	6,342	4,888	−56.7	−36.7	−56.7	−55.8	−34.7	−59.8	−58.4	−38.6	−65.9	9.6	7.7	3.8
6	None known	0	6,932	9,406	−146.4	−3.3	45.0	−154.2	−8.4	45.3	−147.3	−9.9	52.2	9.8	9.9	9.2
7	None	0	8,138	5,645	−33.0	−28.1	42.3	−24.3	−37.8	41.7	−38.2	−30.3	43.8	5.8	16.0	13.1
8	None	0	9,400	3,827	−166.5	246.3	112.9	−175.2	246.0	111.1	−169.3	246.1	110.1	3.9	6.0	8.9
9	None	5	9,629	5,339	−60.2	−18.8	−47.1	−60.9	−22.5	−43.1	−56.9	−20.7	−48.0	3.9	6.6	5.5
10	None	0	12,771	6,197	−29.4	272.1	185.4	−41.4	260.7	192.3	−27.7	268.3	188.6	5.2	16.1	17.9
11	None	1	14,844	9,720	−69.8	16.4	53.8	−69.5	18.5	50.8	−73.2	12.3	54.0	5.4	7.9	3.7
12	None known	0	15,386	8,448	−52.3	0.1	−74.5	−52.8	−0.1	−76.6	−50.6	−0.8	−73.2	2.2	4.0	2.1
13	None	0	18,025	9,551	22.3	−27.5	−100.1	12.2	−59.9	−97.0	22.6	−28.2	−92.5	7.6	33.6	34.0
14	None	0	120,008	154,867	−75.6	−13.8	52.1	−77.7	−13.1	52.0	−77.2	−14.5	54.3	2.8	2.7	2.2

*Method A.
†Method B.
EM = emission; TR = transmission.

obtained with the subjects in the arms-down position. The filtered backprojection reconstructed attenuation scans from these datasets were calculated without segmentation.

CT imaging was performed using a 9800 Advantage or Hi-Speed scanner (General Electric Medical Systems, Milwaukee, WI). Each slice was reconstructed to a 512 × 512 matrix. CT voxel size was $x^2 \cdot 10$ mm^3, where x varied from 0.68 to 0.80 mm depending on the field of view selected for the particular patient. All 14 CT scans were acquired using a no-contrast, arms-down, free-breathing, research protocol.

Registration

The algorithm, MIAMI Fuse (mutual information–based automatic multimodality image fusion), has been applied across a broad spectrum of volume datasets of various modalities and anatomies (*5*). The algorithm requires little or no preprocessing, requires minimal user interaction (user removal of external body tissues is never required), and implements either affine or thin-plate spline warping registration. The process is implemented by allowing an optimizer, the Nelder–Mead simplex algorithm, to drive the positions of control points in the homologous floating dataset—that is, the data volume to be mapped onto the reference volume—to maximize the resultant mutual information between the reference volume and the transformed homologous volume. The optimization routine determines the transformation geometry model's coefficients for a coordinate mapping using the vector of optimizer-specified control points in the homologous volume and the fixed corresponding control points in the reference volume and performs trilinear interpolation to map gray-scale values of the homologous image voxels onto the reference image voxels. The mutual information cost metric is computed from the bivariate histogram of gray values in the reference and reconstructed homologous dataset for geometrically corresponding voxels. Each optimization cycle is initiated by a random perturbation of the initial transformation vector to create the initial simplex needed for the Nelder–Mead algorithm. MIAMI Fuse uses repeated optimizations to maximize mutual information and avoid local optima. For this specific project the process requires the user's placement of only 9 control points in the patient's reference dataset and 3 control points in the homologous data. The 9 control points in the reference were placed at the apices of 3 alternating, inverted axial triangles: 1 more cranial, 1 midplane, and 1 more caudal. These 9 control points are placed without regard to their possible homologous loci in the floating volume. Then 3 control points were picked in the floating volume that are crudely homologous to the first 3 points placed in the reference volume. The ability to reduce the initial registration task of the operator is achieved using an easily edited software schedule to control most aspects of the registration. More specifically, for each registration the algorithm begins using an initial rigid-body geometry model to approximately register the 2 datasets. A 2-stage registration schedule was implemented. In a scale space approach, the initial rigid-body registration uses a reference volume decimated by 50% in all axes to reduce computation time in the initial stage. Criteria for convergence for this initial stage are also less stringent than that used in the final stage described below. After the initial crude, rigid-body registration process finishes, all 9 points in the reference volume are mapped into the floating homologous volume to provide an initialization of the 9-point thin-plate spline warping used in the final registration stage.

PET tumor segmentation was determined by a semiautomated image-intensity thresholding method that identified tumor voxels with intensity greater than 3 SDs above background level in the attenuation-corrected emission dataset that is warped onto the CT volume (*4*). CT tumor segmentation was performed manually by an expert radiologist who was blinded to the PET segmentation. For both modalities the centroid of the segmented region was computed as an intensity-weighted measure—that is,

$$a_c = \sum^{VOI} w_i a_i / \sum^{VOI} w_i,$$

where a_c is the computed *x*-, *y*-, or *z*-centroid-coordinate; a_i is the *x*-, *y*-, or *z*-coordinate, respectively, of the *i*th voxel; and w_i is its amplitude (gray-scale value). The computation of the centroids is limited to the regions segmented by the user on CT or the thresholded region in PET. Intensity weighting potentially further reduces any unintended bias of the manual expert definition.

RESULTS

The results for each of the 14 subjects are presented in Table 1. A summary of the results presented in Table 2 shows that there is a significant difference at $P < 0.01$ between the errors measured by the 2 methods. Note that for method A (the indirect method where the CT is warped onto the PET transmission scan and then the patient's attenuation-corrected emission dataset is substituted for the transmission dataset), there is less difference between the mean and the median (median is 3 SEM below the mean) than for method B (the direct method where the difference is larger) (median is 5 SEM below the mean). These differences are primarily due to disparate results for 3 of the 14 subjects (i.e., subjects 7, 10, and 13, for whom the differences between the 2 methods are dramatic).

DISCUSSION

The improved accuracy obtained by first mapping CT onto the PET attenuation reconstruction likely results from the improved capture range of the algorithm when using 2 attenuation datasets (i.e., CT and PET attenuation). Stated

TABLE 2
Statistical Comparison Between 2 Methods

Method	SEM (mm)	Mean error (mm)	Median error (mm)	F test between methods
Indirect (A)				
EM mapped onto CT using mapping computed from TR mapped onto CT	0.29	6.22	5.31	$P = 0.0064$
Direct (B)				
EM mapped directly onto CT	0.66	10.60	7.12	

EM = emission; TR = transmission.

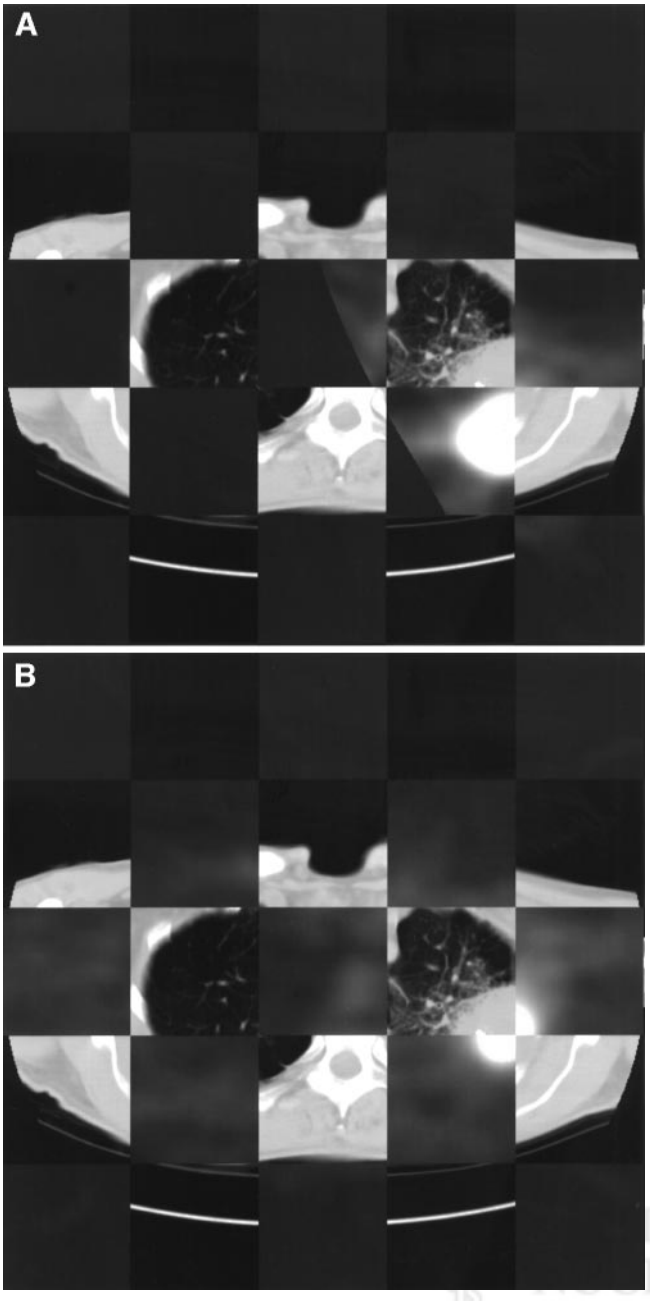

FIGURE 1. (A) One slice of dataset for subject 13 shows failure of direct method. (B) Same CT slice (and subject) as in A shows success of indirect method.

another way, the increased number of outliers of the direct registration of CT data onto PET ^{18}F-FDG attenuation-corrected, emission reconstructions is likely due to the failure of the algorithm to capture the true solution from the initialized starting-pose differences between the 2 datasets. The reconstructed attenuation scan has a generally higher signal-to-noise ratio than the attenuation-corrected emission reconstruction except in the region of the lesion. Of particular importance is the ^{18}F-FDG-poor and noisy signal in the body wall of the normal thorax that must register with the CT body wall.

Figure 1 shows both poor and good registrations for subject 13. The method of displaying the registration in Figure 1 uses a checkerboard of blocks of data from alternate datasets. The sharp, curved line of the ^{18}F-FDG PET in Figure 1A simply indicates the end of the superior extension of the PET emission dataset for this computed mapping. CT voxels to the reader's left of this line map to loci above the maximum superior extent of the PET dataset, whereas voxels to the reader's right map into the PET volume.

The more accurate mapping shown in Figure 1B maps no CT voxels in this slice to PET loci that are out of the acquisition volume; thus, no such boundary is visible. The right half of Figure 1A illustrates the poor registration of the anterior body wall resulting from the method of mapping CT directly onto the PET attenuation-corrected emission data for subject 13 (Table 1). Note how the PET maps posteriorly in the region of the left chest wall leaving the posterior PET emission data mapped onto the supporting table beneath the patient. In Figure 1B, the body wall is more accurately mapped. Issues that affect the capture behavior of the algorithm include how the algorithm treats nonoverlapping, zero-valued voxels. The registrations presented in Figure 1 were made with the algorithm ignoring nonoverlapping voxels where either voxel is zero.

CONCLUSION

Although the algorithm used is fully capable of multimodality registration, the more accurate warping method shown here results from the registration of CT and PET attenuation scans. This method appears preferable for PET/CT fusion in the thorax. Additional studies of the abdomen will be required. The use of such methods may be needed in correcting for respiration artifacts encountered in combined PET/CT scanners currently becoming available.

ACKNOWLEDGMENT

This work was supported by Department of Health and Human Services, Public Health Service, National Institutes of Health grants 1R01CA59412 and 1R01CA52880.

REFERENCES

1. Wahl RL, Quint LE, Cieslak RD, et al. Anatometabolic tumor imaging: fusion of FDG PET with CT or MRI to localize foci of increased activity. *J Nucl Med.* 1993;34:1190–1197.
2. Woods RP, Grafton ST, Watson JDG, Sicotte NL, Mazziotta JC. Automated image registration. II. Intersubject validation of linear and nonlinear models. *J Comput Assist Tomogr.* 1998;22:153–165.
3. Collins DL, Evans AC. Animal: validation and applications of nonlinear registration-based segmentation. *Int J Pat Recog Artif Intel.* 1997;11:1271–1294.
4. Zasadny K, Kison P, Francis I, Wahl R. FDG-PET determination of metabolically active tumor volume and comparison with CT. *Clin Positron Imaging.* 1998;1:123–129.
5. Meyer CR, Boes JL, Kim B, et al. Demonstration of accuracy and clinical versatility of mutual information for automatic multimodality image fusion using affine and thin plate spline warped geometric deformations. *Med Image Anal.* 1997;1:195–206.

JNM The Journal of NUCLEAR MEDICINE

Comparison of Mutual Information-Based Warping Accuracy for Fusing Body CT and PET by 2 Methods: CT Mapped onto PET Emission Scan Versus CT Mapped onto PET Transmission Scan

Joseph Skalski, Richard L. Wahl and Charles R. Meyer

J Nucl Med. 2002;43:1184-1187.

The Journal of Nuclear Medicine is published monthly.
SNMMI | Society of Nuclear Medicine and Molecular Imaging
1850 Samuel Morse Drive, Reston, VA 20190.
(Print ISSN: 0161-5505, Online ISSN: 2159-662X)

SNMMI SOCIETY OF NUCLEAR MEDICINE AND MOLECULAR IMAGING